PAPER

Check for updates

Investigating the magnetic and magnetocaloric behaviors of LiSm(PO$_3$)$_4$

T. A. Tran, [a] Dimitar N. Petrov, [b] T. L. Phan, *[cd] B. D. Tu, [c] H. N. Nhat, [c] H. C. Tran, [a] B. Weise, [e] J. Cwik, [f] Yu S. Koshkid'ko, [f] T. V. Manh, [g] T. P. Hoang [hi] and N. T. Dang *[hj]

We report a detailed study on the magnetic behaviors and magnetocaloric (MC) effect of a single crystal of lithium samarium tetraphosphate, LiSm(PO$_3$)$_4$. The analyses of temperature-dependent magnetization data have revealed magnetic ordering established with decreasing temperature below T_p, where T_p is the minimum of a dM/dT vs. T curve and varies as a linear function of the applied field H. The Curie temperature has been extrapolated from $T_p(H)$ data, as $H \to 0$, to be about 0.51 K. The establishment of magnetic-ordering causes a substantial change in the heat capacity C_p. Above T_p, the crystal exhibits paramagnetic behavior. Using the Curie–Weiss (CW) law and Arrott plots, we have found the crystal to have a CW temperature $\theta_{CW} \approx -36$ K, and short-range magnetic order associated with a coexistence of antiferromagnetic and ferromagnetic interactions ascribed to the couplings of magnetic dipoles and octupoles at the Γ_7 and Γ_8 states. An assessment of the MC effect has shown increases in value of the absolute magnetic-entropy change ($|\Delta S_m|$) and adiabatic-temperature change (ΔT_{ad}) when lowering the temperature to 2 K, and increasing the magnetic-field H magnitude. Around 2 K, the maximum value of $|\Delta S_m|$ is about 3.6 J kg^{-1} K^{-1} for the field $H = 50$ kOe, and ΔT_{ad} is about 5.8 K for $H = 20$ kOe, with the relative cooling power (RCP) of ~82.5 J kg^{-1}. In spite of a low MC effect in comparison to Li(Gd,Tb,Ho)(PO$_3$)$_4$, the absence of magnetic hysteresis reflects that LiSm(PO$_3$)$_4$ is also a candidate for low-temperature MC applications below 25 K.

1. Introduction

The magnetocaloric (MC) effect is an intrinsic property of any magnetic material. It is related to a temperature change of a magnetic material under an adiabatic process when an external magnetic field is applied. This phenomenon is generated from a decreased magnetic entropy that is compensated by the lattice-entropy change because the total entropy of the system under an isentropic process is unchanged. Together with the isentropic process, an adiabatic process also takes place irreversibly, after in the entropy–temperature (S–T) diagram.[1] In other words, the isentropic change of the material leads to an adiabatic temperature change (ΔT_{ad}), and when the magnetization is isothermally carried out, a magnetic-entropy change (ΔS_m) causes an isothermal total entropy change.[1–3] Using the adiabatic demagnetization and paramagnetic (PM) salts, typically Gd$_2$(SO$_4$)$_3 \cdot$8H$_2$O, (Dy,Ce)(C$_2$O$_5$SO$_4$)$_3 \cdot$9H$_2$O and (NH$_4$)$_2$SO$_4$MnSO$_4 \cdot$6H$_2$O, one has been given the birth of cryogenic and sub-Kelvin cooling.[1,4,5] The successful fabrication of adiabatic demagnetization refrigerators can somewhat solve the shortage and high price of ^{3}He helium isotope.[6]

Comparing with the vapor-compression refrigeration cycle, the MC-based refrigeration has been proven to gain a higher efficiency,[7] and does not cause environmental challenges because of using recyclable solid refrigerants composed of non-toxic elements.[1,8] Apart from using PM salts, it has been seeking for H$_2$O-free MC materials applicable for sub-Kelvin/cryogenic cooling devices[1,4,5] and space technology,[9] particularly for the liquefaction of hydrogen and helium isotopes at below 20 and 4.2 K, respectively. These materials need to ensure some application requirements, such as low magnetic-ordering

[a]Department of Physics, Ho Chi Minh City University of Technology and Education, 700000 Hochiminh, Vietnam

[b]Department of Physical Chemistry, Plovdiv University "Paisii Hilendarski", 24 Tzar Asen Str., 4000 Plovdiv, Bulgaria

[c]Faculty of Engineering Physics and Nanotechnology, VNU-University of Engineering and Technology, 144 Xuan Thuy, Cau Giay, Hanoi, Vietnam. E-mail: ptlong2512@yahoo.com

[d]Department of Physics and Oxide Research Center, Hankuk University of Foreign Studies, Yongin 449-791, South Korea

[e]Leibniz IFW Dresden, Institute for Complex Materials, D-01069, Dresden, Germany

[f]Institute of Low Temperature and Structure Research, PAS, Okólna 2, 50-422 Wroclaw, Poland

[g]Phenikaa University Nano Institute (PHENA), Phenikaa University, Hanoi 12116, Vietnam

[h]Faculty of Environmental and Natural Sciences, Duy Tan University, 550000 Danang, Vietnam. E-mail: dangngoctoan1@duytan.edu.vn

[i]Laboratory Center, Duy Tan University, 550000 Danang, Vietnam

[j]Institute of Research and Development, Duy Tan University, 550000 Danang, Vietnam

temperature, large $|\Delta S_m|$ and ΔT_{ad} values, no thermal hysteresis phenomenon, and no degrading at high temperatures and ultra-high vacuum. Until now, it has been introduced many materials with magnetic-ordering temperatures below 20 K satisfying with the above requirements, such as Re(V, P)O$_4$ zircon-type oxides (Re is a rare-earth element),[9–12] ReMO$_3$ perovskite-type oxides (M is a transition metal),[13–16] EuRe$_2$O$_4$ spinel-type oxides,[17,18] Re$_3$CrGa$_4$O$_{12}$ garnets,[19,20] KBaYb(BO$_3$)$_2$,[21] and many alloys (including ErMn$_2$Si$_2$,[22] Er$_2$Ni$_{1.5}$Ga$_{2.5}$,[23] Er$_3$Ni$_6$-Al$_2$,[24] Ho$_2$Ni$_{0.95}$Si$_{2.95}$,[25] and YbPt$_2$Sn[26]), in which YbPt$_2$Sn[26] could work from 2 K down to 0.2 K. Recently, Petrov et $al.$[27] have found a large MC effect in LiRe(PO$_3$)$_4$ single crystals (Re = Gd, Tb, and Dy), a material system has been widely used for optoelectronic applications.[28–30] Intriguing optical and magnetic properties of these LiRe(PO$_3$)$_4$ materials are related to Re^{3+} ions confined in the ReO$_8$ dodecahedral crystal field. In crystallography, along the b axis, edge-shared ReO$_8$ dodecahedra and LiO$_4$ tetrahedra in turn arrange, while PO$_4$ tetrahedra form helical chains. Additionally, the ReO$_8$ and LiO$_4$ chains share their corners with the helical PO$_4$ chains that constitute a 3D framework.[31,32] Together with the 3D framework, a large nearest Re–Re distance ($\sim$5.6 Å[31,33]) is thought to obstruct exchange interactions between Re ions, leading to a large MC effect of LiRe(PO$_3$)$_4$ at low temperatures. Investigating LiRe(PO$_3$)$_4$ materials with Re = Gd, Tb, Dy and Pr, Petrov et $al.$[27,32] found their $|\Delta S_m|$ and ΔT_{ad} values at 2 K are about 9.8–27.6 J kg^{-1} K^{-1} for the field $H = 50$ kOe and 3–13 K for $H = 20$ kOe, respectively.

To learn more about this LiRe(PO$_3$)$_4$ material system, we have prepared a single crystal of lithium samarium tetraphosphate, LiSm(PO$_3$)$_4$, and investigated in detail its structural characterization, magnetic behaviors and MC effect. To the best of our knowledge, no previous work on the magnetocaloric behaviors of LiSm(PO$_3$)$_4$, though its electronic and optical properties have been widely studied.[34–36] Herein, the magnetic behaviors have studied through the magnetization (M) and heat-capacity (C_p) measurements $versus$ the temperature and magnetic field. Based on these M and C_p data, and thermodynamic relations, the characteristic parameters of the MC effect ($|\Delta S_m|$ and ΔT_{ad}) have been evaluated in comparison to the previous works on low-temperature MC materials.

2. Experimental details

A single crystal (SC) of LiSm(PO$_3$)$_4$ was grown by using the flux method.[37] After fabrication, its crystal structure was analyzed by using an X-ray diffractometer in Bragg–Brentano geometry (Malvern Panalytical) equipped with an X-ray wavelength of 1.5406 Å. To record the magnetization and heat-capacity data dependent on the temperature and magnetic field, $M(T, H)$ and $C_p(T, H)$, respectively, we used a Quantum Design Physical Properties Measurement System (PPMS-9). Specifically, $M(T, H)$ data were recorded at temperatures $T = 2$–300 K and magnetic fields $H = 0$–50 kOe, while $C_p(T, H)$ data were recorded at $T = 2$–300 K and $H = 0$–20 kOe. After collecting $M(T, H)$ and $C_p(T, H)$ data, $|\Delta S_m(T, H)|$ and ΔT_{ad} were calculated by using Maxwell's relations and thermodynamic equations.
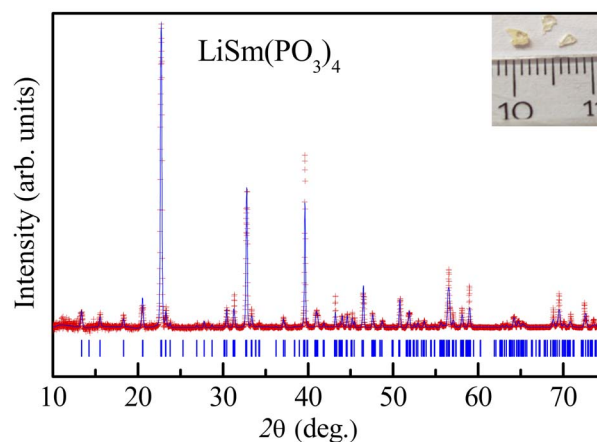

Fig. 1 Room-temperature XRD pattern of LiSm(PO$_3$)$_4$. Experimental data (red symbols) and calculated profile (blue lines) are shown. Vertical blue ticks denote the nuclear reflections of the monoclinic C2/c phase. The inset shows an image of LiSm(PO$_3$)$_4$ single crystals studied in this work.

3. Results and discussion

The LiSm(PO$_3$)$_4$ SC after fabricated has pale yellow (see the inset of Fig. 1), which was roughly ground to examine the structural properties by using the X-ray diffraction (XRD) method. The X-ray data analysis based on the profile matching mode (Le Bail fit) belonging to the FullProf structural refinement software[38] has revealed that the diffraction peaks can be fitted successfully only with a monoclinic phase with the C2/c symmetry, indicating a single-phase nature of our sample. The refined lattice parameters, $a = 16.3784(7)$ Å, $b = 7.0373(6)$ Å, $c = 9.6895(5)$ Å, and $\beta = 126.071(3)°$, are well consistent with those obtained from previous works on LiSm(PO$_3$)$_4$.[39,40]

Following the structural characterization, we have studied the magnetic behaviors of LiSm(PO$_3$)$_4$ upon analyzing $M(T, H)$ and $C_p(T, H)$ data. In Fig. 2, it graphs $M(T)$ data measured for the sample in powder according to the increasing and decreasing directions of temperature for an applied field $H = 1$ kOe. Similar to Li[Gd,Tb,Dy](PO$_3$)$_4$ (ref. 27) and (Er,Yb)VO$_4$ (ref. 9) materials, we have also observed a gradual decrease in M when T increases from 2 to $\sim$300 K. Though T reached 2 K, no trace of magnetic-ordering transition temperatures (Néel/Curie temperatures, T_N/T_C) was observed. The performance of the magnetic susceptibility ($\chi^{-1} = H/M$) from these $M(T)$ data, and the extrapolation of the high-temperature Curie–Weiss (CW) law would obtain the CW temperature (θ_{CW}) of about -36 K, as shown in Fig. 2. A negative θ_{CW} value reflects that antiferromagnetic (anti-FM) super-exchange interactions take place between Sm^{3+} ions in SmO$_8$ chains of monoclinic LiSm(PO$_3$)$_4$ mediated by O and P ions. In other words, LiSm(PO$_3$)$_4$ is anti-FM with the Néel temperature (T_N) lower than 2 K. Measuring a full $M(H)$ loop at 2 K, we have found no magnetic hysteresis. M tends to saturate as $H > 10$ kOe, with a saturation value (M_s) of $\sim$22.4 emu g^{-1} (or $\sim$1.97 μ_B/f.u.), see the inset of Fig. 2. This effective moment value is fairly greater than the theoretical value of $g_J[J(J + 1)]^{1/2} =$

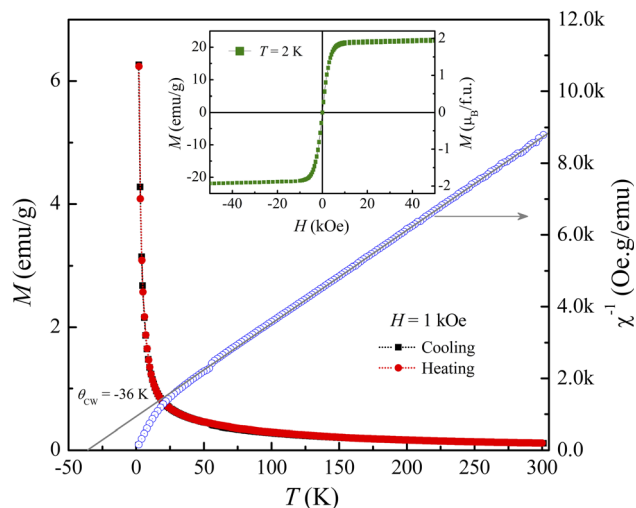**Fig. 2** $M(T)$ and $\chi^{-1}(T)$ curves of LiSm(PO$_3$)$_4$ in the field $H = 1$ kOe, and the straight line is plotted according to the CW law. The inset is an $M(H)$ loop recorded at $T = 2$ K.

$0.85\mu_B$ for a free Sm^{3+} ion in the ground state ($4f^5$, $^6H_{5/2}$, with $S = 5/2$, $L = 5$ and $J = L - S$), and experimental values obtained for Sm^{3+} in van-Vleck-paramagnetic compounds of Sm$_3$Sb$_3$Zn$_2$O$_{14}$ (ref. 41) and SmZnAl$_{11}$O$_{19}$.[42] Such differences could be due to the fact that Sm^{3+} is a Kramers ion and occupies in various crystal fields. In the SmO$_8$ dodecahedral field, there could be a degenerate ground state with several types of degrees of freedom. After the ground term $^6H_{5/2}$, the next higher order term, $J = L - S + 1$ ($^6H_{7/2}$), has a moment value of $3.32\mu_B$. Energy

levels of these terms seem close to each other, and can mix as a function of T and H. Additionally, due to the crystalline-electric-field effect, a $J = 5/2$ ground state can split into a Γ_7 doublet and a Γ_8 quartet. The Γ_7 state has a magnetic dipole while the Γ_8 state has a magnetic dipole, electric quadrupoles and magnetic octupoles.[43] The interactions of magnetic dipoles and octupoles could result in a large value of magnetic moment of LiSm(PO$_3$)$_4$. As studying the materials having strongly-correlated electron states *via* hybridization with electrons, it has also been found large magnetic moments of $1.2–1.7\mu_B$.[43] Measuring a series of $M(T)$ curves at higher fields $H = 2–50$ kOe and $T = 2–50$ K, as shown in Fig. 3(a), we have found a gradual increase of paramagnetic background signals, and M becomes saturated at $M_s \sim 22.4$ emu g^{-1} as $H \geq 10$ kOe. There is a temperature range (named a saturation region) from 2 K that M is less changed and approximately equal to M_s. It broadens towards high temperatures when H increases above 30 kOe, see a dashed rectangle plotted in Fig. 3(a). After the saturation region, M would gradually decrease with increasing T. Interestingly, having performed d$M(T)$/dT data, we have observed the minimum that starts appearing as $H \approx 5$ kOe at the so-called T_p temperature. T_p tends to shift towards higher temperatures as increasing H, see Fig. 3(b) and its inset. This proves an H-dependent ferromagnetic–paramagnetic (FM–PM) separation at T_p. These $T_p(H)$ data can be described a linear function of $T_p = 0.51 + 0.48 \times H$, as shown in Fig. 4. The zero-field extrapolation, $H \rightarrow 0$, would obtain the Curie temperature (T_C) of LiSm(PO$_3$)$_4$ at 0.51 K. A negative θ_{CW} value together with these results suggest a coexistence of FM and anti-FM interactions induced by Sm^{3+} ions (probably associated with interactions between magnetic dipoles and octupoles of the Γ_7 and Γ_8 states) in LiSm(PO$_3$)$_4$ at low temperatures and fields. The high-field application promotes FM-ordering establishment, leading to the FM–PM transition at T_p. It is necessary to measure $M(T, H)$ data at lower temperatures (<2 K) to identify exactly LiSm(PO$_3$)$_4$ being a ferromagnet and/or antiferromagnet.
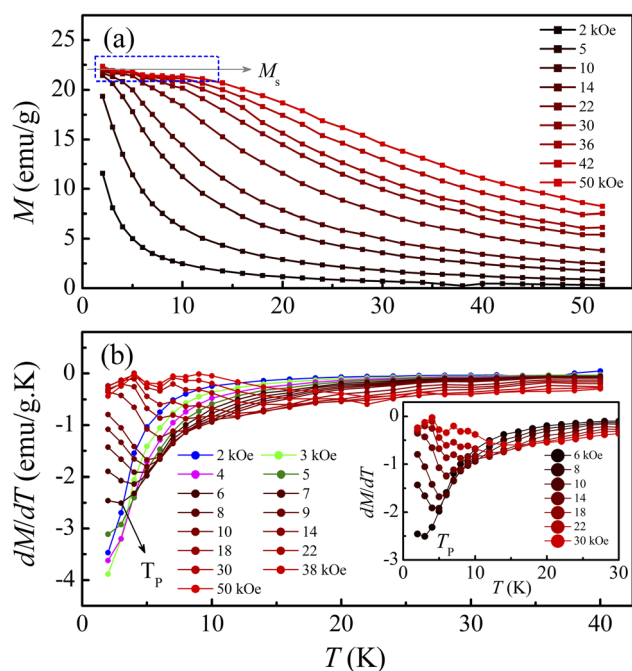

Fig. 3 (a) $M(T)$ and (b) d$M(T)$/dT data of LiSm(PO$_3$)$_4$ in different applied fields of $H = 2–50$ kOe. The inset plots an enlarged view of the d$M(T)$/dT data for $H = 6–30$ kOe showing the minima at T_p.

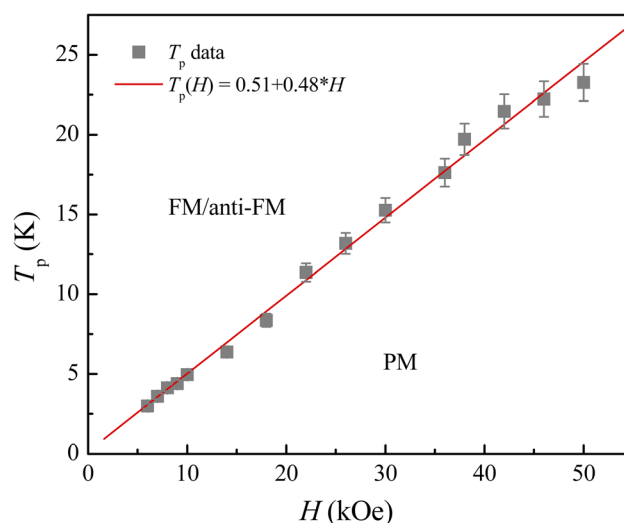**Fig. 4** H-Dependent T_p data of LiSm(PO$_3$)$_4$ showing a FM–PM phase separation.

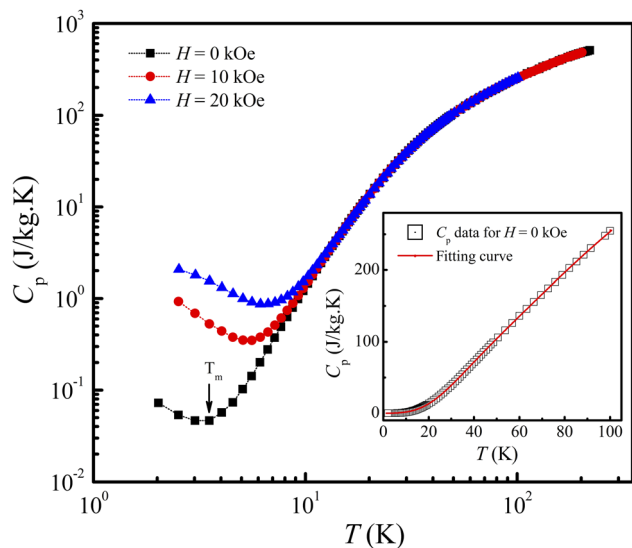**Fig. 5** $C_p(T)$ data of LiSm(PO$_3$)$_4$ in the log−log scale for H = 0, 10, and 20 kOe. The insets plots $C_p(T)$ data for H = 0 fitted to a combination of Debye−Einstein functions, eqn (1).

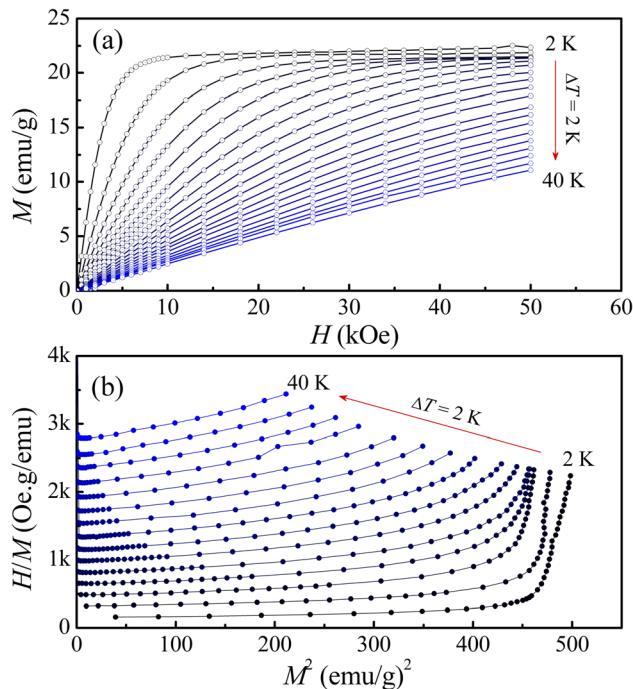**Fig. 6** (a) Representative $M(H)$ and (b) $M^2(H/M)$ data of LiSm(PO$_3$)$_4$ at temperatures T = 2−40 K, where temperature increments are maintained at 2 K.

The FM-ordering establishment in the LiSm(PO$_3$)$_4$ sample can be further confirmed upon $C_p(T)$ measurement at different applied fields for a bulk sample. The $C_p(T, H)$ data for H = 0–20 kOe graphed in Fig. 5 indicate a gradual decrease of C_p as decreasing T from 300 K to T_m, which is defined as the point that a decrease in temperature below it will enhance C_p. T_m is about 3.7 K for H = 0 and increases to ∼6.7 K for H = 20 kOe. An enhancement of C_p as lowering T below T_m is assigned to the magnetic contribution to heat capacity,[44] demonstrating the establishment of magnetic ordering in this material. Due to the limit of low-temperature measurement, we could not obtain the onset of magnetic ordering (i.e., T_N or T_C) corresponding to a (Schottky) peak in the $C_p(T, H)$ curves such as phenomena observed in materials GdVO$_4$,[9] (Tb,Dy,Ho)$_3$CrGa$_4$O$_{12}$,[19] Li(Gd,Tb,Dy)(PO$_3$)$_4$,[27] and ErRuSi.[44] It should be noticed that the magnetic contribution to C_p is mainly at temperatures below T_m. Above T_m, the phonon contribution (C_{ph}) to C_p plays a dominant role, consequently C_p is less dependent on H. We have found that the $C_p(T)$ data for H = 0 and T = 2–100 K can be described by the combination of one Debye and one Einstein terms for phonons:[45]

$$C_{ph} = m\left[9R\left(\frac{T}{\theta_D}\right)^3 \int_0^{\frac{\theta_D}{T}} \frac{x^4 e^x}{(e^x - 1)^2}\,dx\right]$$
$$+ n\left(\frac{\theta_E}{T}\right)^2 \frac{\exp\left(\frac{\theta_E}{T}\right)}{\left(\exp\left(\frac{\theta_E}{T}\right) - 1\right)^2}, \tag{1}$$

see the inset of Fig. 5, where θ_D is the Debye temperature, θ_E is the Einstein temperature, and m and n are the fit parameters. The sum $m + n$ was fixed to the total number of atoms in the formula unit of LiSm(PO$_3$)$_4$. Herein, the obtained values of θ_D and θ_E are about 217.6 and 439.4 K, respectively.

Magnetic behaviors of LiSm(PO$_3$)$_4$ can be further understood as considering $M(H)$ isotherms recorded at T = 2−50 K. Typical $M(H)$ curves shown in Fig. 6(a) indicate the change in their curvature when T increases from 2 to 40 K, particularly at fields H = 0–20 kOe. In other words, low-temperature nonlinear $M(H)$ curves become linear as increasing T above 30 K. This indicates the collapse of magnetic ordering, and the material becomes paramagnetic at high temperatures. Similar to $M(T)$ data shown in Fig. 3(a), below 8 K, M goes to saturate as raising H above 30 kOe. As performing $M^2(H/M)$ plots, see Fig. 6(b), it comes to our attention that these curves have positive slopes, and are not parallel straight lines. These features reflect that LiSm(PO$_3$)$_4$ undergoes a second-order nature in the investigating temperature range (according to Banerjee's criteria[46]) and exhibiting short-range magnetic order (according to Arrott and Noakes[47,48]). Short-range magnetic order in LiSm(PO$_3$)$_4$ is ascribed to a coexistence of FM and anti-FM interactions between Sm^{3+} ions via O and P atoms. Additionally, under the impacts of the crystal and magnetic fields, Kramers doublet on Sm^{3+} ions could have more ($2J + 1$)-fold degeneracy, leading to multiplets.[32] The jj-coupling and/or spin population on these multiplets could also cause short-range magnetic order in LiSm(PO$_3$)$_4$.

Together with the magnetic behaviors, we have also studied the MC effect through the parameters $|\Delta S_m|$ and ΔT_{ad} calculated by the following expressions:[1]

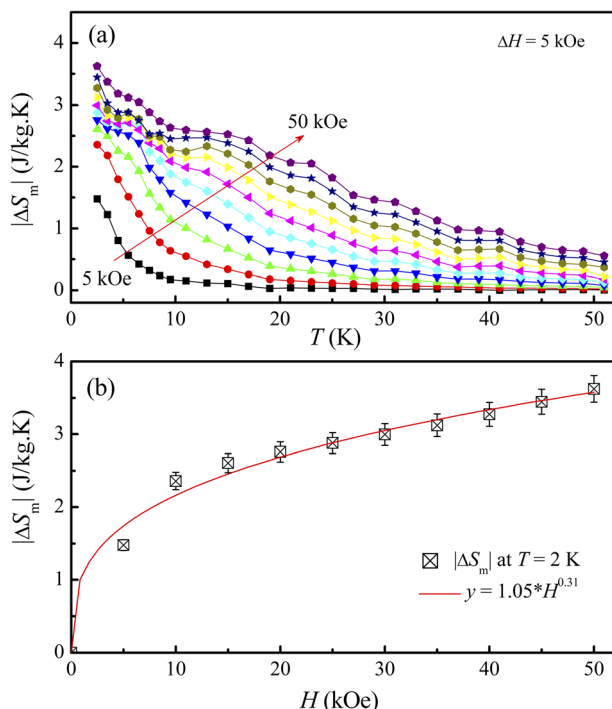$$|\Delta S_m(T, H)| = \int_0^H \left(\frac{\partial M}{\partial T}\right)_H dH \tag{2}$$

Fig. 7 (a) $|\Delta S_m(T)|$ data of LiSm(PO$_3$)$_4$, and (b) $|\Delta S_m(H)|$ data at $T = 2$ K fitted to a function $y = a \times H^n$.

$$\Delta T_{ad} = \frac{T}{C_p(T, H)}|\Delta S_m(T, H)|. \qquad (3)$$

Fig. 7(a) shows $|\Delta S_m|$ data of LiSm(PO$_3$)$_4$ at temperatures $T = 2$–50 kOe in magnetic fields $H = 5$–50 kOe, with magnetic-field increments (ΔH) fixed at 5 kOe. One can see that $|\Delta S_m(T)|$ increases with increasing H, particularly at $T < 25$ K. Due to magnetic saturation, $|\Delta S_m(T)|$ less changes at high fields (>30
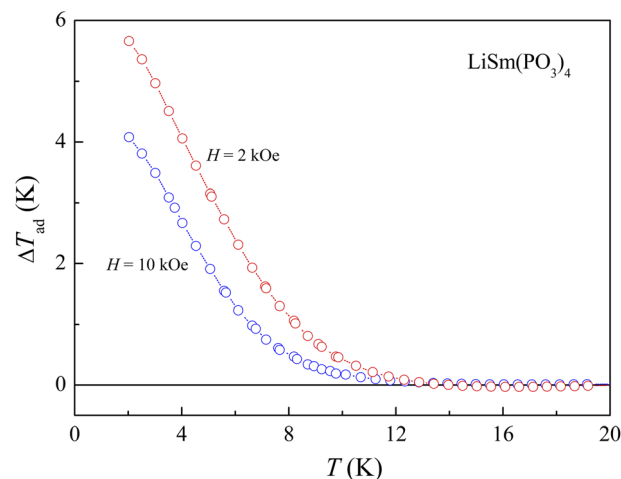

Fig. 9 $\Delta T_{ad}(T)$ calculated from $C_p(T, H)$ data of LiSm(PO$_3$)$_4$ for $H = 10$ and 20 kOe, using eqn (3).

kOe). At $T = 2$ K, $|\Delta S_m|$ is largest ($|\Delta S_{max}|$) of ~3.6 J kg^{-1} K^{-1} for $H = 50$ kOe. This value is fairly smaller than the $|\Delta S_m|$ values (9.8–27.6 J kg^{-1} K^{-1}, $H = 50$ kOe) obtained for Li(Gd,Tb,Dy,Pr)(PO$_3$)$_4$ single crystals.[27,32] It is reasonable because magnetic moment of Sm^{3+} is lower than that of Gd^{3+}, Tb^{3+}, Dy^{3+}, and Pr^{3+}.[49] Considering $|\Delta S_m(H)|$ data at $T = 2$ K, we have found that these data could be described by a power law of $y = a \times H^n$, with $a = 1.05$ and $n = 0.31$. This n value falls in the range of Li(Gd,Tb,Dy)(PO$_3$)$_4$ materials with $n = 0.12$–0.64,[27] but smaller than the value of mean-field theory (MFT) $n = 0.67$.[8] According to Franco et al.,[8] n has a relationship with another parameter $N(T, H)$ characteristic for magnetic ordering, which is calculated as follows:

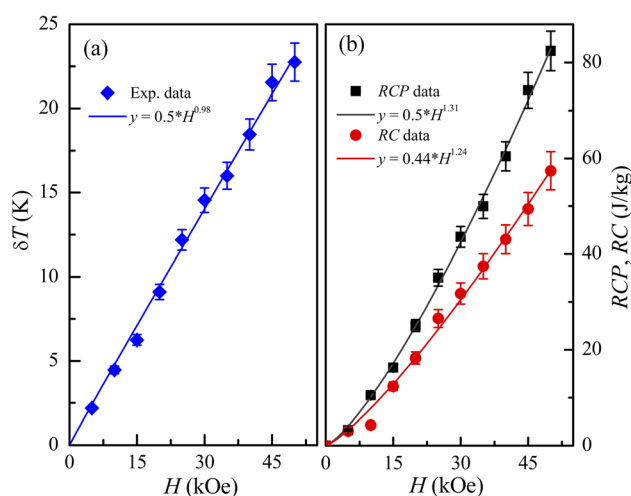$$N(T, H) = \frac{d \ln|\Delta S_m(T, H)|}{d \ln H}. \qquad (4)$$

Fig. 8 $N(T, H)$ data of LiSm(PO$_3$)$_4$ for $H = 5$–50 kOe calculated by using eqn (4).

Fig. 10 (a) $\delta T(H)$ and (b) RCP(H) and RC(H) data of LiSm(PO$_3$)$_4$ for $H = 0$–50 kOe fitted to a power law of $y = b \times H^m$, with the values of b and m labeled in the figures.

Table 1 MC behaviors of LiSm(PO$_3$)$_4$ and typical MC materials with T_N (T_C) < 10 K at H = 50 kOe

Compound	T_N/T_C (K)	$|\Delta S_{max}|$ (J kg^{-1} K^{-1})	RCP/RC (J kg^{-1})	Ref.
LiSm(PO$_3$)$_4$	/0.51	3.6	82.4/57.4	This work
LiGd(PO$_3$)$_4$	—	27.6	174/133	27
LiTb(PO$_3$)$_4$	—	15.9	334/254	27
LiDy(PO$_3$)$_4$	—	11.7	236/193	27
NaGdF$_4$	2.3	51.2	331/250	50
DyVO$_4$	3.5	19.8	∼300	51
EuSe	4.6	37.5	580	52
EuTiO$_3$	4.4–5.6	40.4–42.2	300–353	14
ErRu$_2$Si$_2$	5.5	17.6	278	53

For ferromagnets obeying the MFT (long-range ferromagnets), N goes to 1 and 2 as $T \ll T_C$ and $T \gg T_C$, respectively. It achieves the minimum at $T = T_C$, and $n = N(T_C) = 0.67$, which is independent of H.[8] In our work, though N tends to 2 at high temperatures (corresponding to the paramagnetic region), the minima of $N(T, H)$ are about 0.1–0.2 and strongly dependent on H, which are much lower than the MFT value, as shown in Fig. 8.

This deviation is ascribed to (i) $|\Delta S_m(H)|$ and $N(T, H)$ values calculated at temperatures higher than T_N/T_C, and (ii) the absence of long-range magnetic order in LiSm(PO$_3$)$_4$. If combining $|\Delta S_m(T)|$ and $C_p(T)$ data for H = 0–20 kOe, we would evaluate $\Delta T_{ad}(T)$ values upon eqn (3). As seen in Fig. 9, ΔT_{ad} increases gradually when T decreases below 12 K. The maximum ΔT_{ad} for LiSm(PO$_3$)$_4$ are about 4 and 5.8 K at 2 K, for applied fields of 10 and 20 kOe, respectively, which is higher than the maximum ΔT_{ad} (∼2.8 K) of LiPr(PO$_3$)$_4$ (ref. 32) at the same conditions. For Li(Gd,Tb,Dy)(PO$_3$)$_4$, they have fairly higher maximum ΔT_{ad} values of 11.9–12.9 K at 2 K and H = 20 kOe.[27] These differences are mainly related to the ground-state degeneracy of RE ions due to spin–orbit coupling and impacts of crystal and magnetic fields, depending on each rare-earth ion type.

Together with $|\Delta S_m|$ and ΔT_{ad}, it is also additionally assessed the relative cooling power (RCP) and/or the refrigeration capacity (RC) by using the following expressions:[1,8]

$$\text{RCP} = |\Delta S_{max}| \times \delta T, \tag{5}$$

$$\text{RC} = \int_{T_1}^{T_2} |\Delta S_m(T)| dT, \tag{6}$$

where δT is the full-width-at-half maximum of a $|\Delta S_m(T)|$ curve. Meanwhile, T_1 and T_2 are defined as the cold and hot ends, respectively, of an ideal thermodynamic cycle that are usually selected at the middle points of a $|\Delta S_m(T)|$ curve. With $|\Delta S_m(T)|$ curves shown in Fig. 7(a), one can see their linewidth (δT) increases with increasing H, and $\delta T \approx 23$ K for H = 50 kOe, see Fig. 10(a). In the investigating H range, $\delta T(H)$ dependence is almost linear (described by a function $y \approx 0.5 \times H^{0.98}$). An enhanced δT is expected to increase RCP and RC with respect to H. As shown in Fig. 10(b), both RCP and RC increases according to power functions of H ($y = b \times H^m$, with m = 1.31 and 1.24 for RC and RCP, respectively), in which RCP is about 1.2–1.4 time higher than that of RC. For H = 50 kOe, RCP (RC) is about 82.4 (57.4) J kg^{-1}.

For comparison, we have summarized the MC behaviors ($|\Delta S_{max}|$ and RCP/RC values) of LiSm(PO$_3$)$_4$ compared with those of some typical materials with T_N (T_C) < 10 K, for the field H = 50 kOe. These materials are potential magnetic coolants useable for liquefying helium and hydrogen gases. The data shown in Table 1 reveals that LiSm(PO$_3$)$_4$ has MC values of $|\Delta S_{max}|$ = 3.6 J kg^{-1} K^{-1} and RCP (RC) = 82.4 (57.4) J kg^{-1}. Belonging to the same family, Li(Gd,Tb,Dy)(PO$_3$)$_4$ have larger MC values, with $|\Delta S_{max}|$ = 11.7–27.6 J kg^{-1} K^{-1} and RCP (RC) = 174–334 (133–254) J kg^{-1},[27] which are comparable to MC behaviors of DyVO$_4$ (ΔS_{max} = 19.8 J kg^{-1} K^{-1} and RCP ≈ 300 J kg^{-1})[51] and ErRu$_2$Si$_2$ (ΔS_{max} = 17.6 J kg^{-1} K^{-1} and RCP = 278 J kg^{-1}).[53] It has been found large MC values as studying NaGdF$_4$ ($|\Delta S_{max}|$ = 51.2 J kg^{-1} K^{-1} and RCP (RC) = 331 (250) J kg^{-1}),[50] and EuTiO$_3$ ($|\Delta S_{max}|$ = 40.4–42.2 J kg^{-1} K^{-1} and RCP = 300–353 J kg^{-1}).[14] Studying EuSe, it has found its MC values being very large with $|\Delta S_{max}|$ = 37.5 J kg^{-1} K^{-1} and RCP = 580 J kg^{-1}.[53] Though Sm^{3+}-related MC materials have been less studied, it is clear that LiSm(PO$_3$)$_4$ has fairly humble MC values. We think that spin–orbit interaction (L–S coupling) and the J = 5/2 ground-state degeneracy into the Γ_7 and Γ_8 states lead to a competition of FM and anti-FM interactions between Sm^{3+} ions, meaning short-range magnetic order, consequently low MC effect in LiSm(PO$_3$)$_4$.

4. Conclusion

We recorded XRD, dc magnetization $M(T, H)$, and heat capacity $C_p(T, H)$ data to investigate the magnetic and MC behaviors of LiSm(PO$_3$)$_4$. Rietveld refinement demonstrated a single phase in the $C2/c$ monoclinic structure of LiSm(PO$_3$)$_4$. The analyses of $M(T)$, $M(H)$ and $C_p(T, H)$ data demonstrated the magnetic-ordering establishment at low temperatures, and a coexistence of FM and anti-FM interactions with $\theta_{CW} \approx -36$ K and $T_C \approx 0.51$ K. The FM phase tends to widen towards high temperatures as increasing H. MC assessments based on $|\Delta S_m|$ and ΔT_{ad} indicated an increase of these parameters as lowering T down to 2 K, and increasing the H magnitude. At 2 K, the maximum values of $|\Delta S_m|$, and ΔT_{ad} are about 3.6 J kg^{-1} K^{-1} for H = 50 kOe, and 5.8 K for H = 20 kOe. Thus, the corresponding values of RCP and RC are about 82.5 and 57.4 J kg^{-1} for H = 50 kOe, respectively. It should be noticed that the MC effect of LiSm(PO$_3$)$_4$ is fairly smaller than that of Li(Gd,Tb,Dy)(PO$_3$)$_4$ having the same structure. Strong L–S coupling, the J = 5/2

ground-state degeneracy into the Γ_7 and Γ_8 states, and the competition of FM and anti-FM interactions between Sm^{3+} ions, causing short-range magnetic ordering, are thought to lead to low MC effect of $LiSm(PO_3)_4$.

Author statement

T. A. Tran, Dimitar N. Petrov, N. T. Dang, and T. L. Phan: conceptualization, methodology and writing; T. P. Hoang, H. C. Tran, B. D. Tu, Yu S. Koshkid'ko, B. Weise, and V. M. Tien: investigation and data analyses; and J. Ćwik, and H. N. Nhat: reviewing and editing.

Conflicts of interest

The authors declare that they have no known competing financial interests or personal relationships that could have appeared to influence the work reported in this paper.

Acknowledgements

References

1 A. M. Tishin and Y. I. Spichkin, *The Magnetocaloric Effect and its Applications*, CRC Press, 2003, DOI: 10.1201/9781420033373.

2 V. K. Pecharsky and K. A. Gschneidner, Magnetocaloric effect and magnetic refrigeration, *J. Magn. Magn. Mater.*, 1999, **200**, 44–56, DOI: 10.1016/S0304-8853(99)00397-2.

3 A. Kitanovski, Energy Applications of Magnetocaloric Materials, *Adv. Energy Mater.*, 2020, **10**, 1903741, DOI: 10.1002/aenm.201903741.

4 W. F. Giauque, A thermodynamic treatment of certain magnetic effects. A proposed method of producing temperatures considerably below 1° absolute, *J. Am. Chem. Soc.*, 1927, **49**, 1864–1870, DOI: 10.1021/ja01407a003.

5 W. F. Giauque and D. P. MacDougall, Attainment of temperatures below 1° absolute by demagnetization of $Gd_2(SO_4)_3 \cdot 8H2O$, *Phys. Rev.*, 1933, **43**, 768, DOI: 10.1103/PhysRev.43.768.

6 R. T. Kouzes and J. H. Ely, *PNNL-19360: Status Summary of 3He and Neutron Detection Alternatives for Homeland Security*, Richland, WA (United States), 2010, DOI: 10.2172/981573.

7 J. Lyubina, Magnetocaloric materials for energy efficient cooling, *J. Phys. D: Appl. Phys.*, 2017, **50**, 053002, DOI: 10.1088/1361-6463/50/5/053002.

8 V. Franco, J. S. Blázquez, J. J. Ipus, J. Y. Law, L. M. Moreno-Ramírez and A. Conde, Magnetocaloric effect: From materials research to refrigeration devices, *Prog. Mater. Sci.*, 2018, **93**, 112–232, DOI: 10.1016/j.pmatsci.2017.10.005.

9 K. Dey, A. Indra, S. Majumdar and S. Giri, Cryogenic magnetocaloric effect in zircon-type RVO$_4$ (R = Gd, Ho, Er,

10 Y. Y. Yu, D. N. Petrov, P. T. Long, K. C. Park, J. Ćwik, P. T. Phong and B. T. Huy, Electronic structure and large magnetocaloric effect in GdVO$_4$ nanocrystals, *J. Alloys Compd.*, 2021, **885**, 161002, DOI: 10.1016/j.jallcom.2021.161002.

11 E. Palacios, M. Evangelisti, R. Sáez-Puche, A. J. Dos Santos-García, F. Fernández-Martínez, C. Cascales, M. Castro, R. Burriel, O. Fabelo and J. A. Rodríguez-Velamazán, Magnetic structures and magnetocaloric effect in RVO$_4$ (R = Gd, Nd), *Phys. Rev. B*, 2018, **97**, 214401, DOI: 10.1103/PhysRevB.97.214401.

12 Y. Y. Yu, D. N. Petrov, K. C. Park, B. T. Huy and P. T. Long, Magnetic and cryogenic magnetocaloric properties of GdPO$_4$ nanorods, *J. Magn. Magn. Mater.*, 2021, **519**, 167452, DOI: 10.1016/j.jmmm.2020.167452.

13 S. Mahana, U. Manju and D. Topwal, Giant magnetocaloric effect in GdAlO3 and a comparative study with GdMnO$_3$, *J. Phys. D: Appl. Phys.*, 2017, **50**, 035002, DOI: 10.1088/1361-6463/50/3/035002.

14 A. Midya, P. Mandal, K. Rubi, R. Chen, J. S. Wang, R. Mahendiran, G. Lorusso and M. Evangelisti, Large adiabatic temperature and magnetic entropy changes in EuTiO$_3$, *Phys. Rev. B*, 2016, **93**, 094422, DOI: 10.1103/PhysRevB.93.094422.

15 J. H. Jia, Y. J. Ke, X. X. Zhang, J. F. Wang, L. Su, Y. D. Wu and Z. C. Xia, Giant magnetocaloric effect in the antiferromagnet GdScO$_3$ single crystal, *J. Alloys Compd.*, 2019, **803**, 992–997, DOI: 10.1016/j.jallcom.2019.06.361.

16 M. Balli, B. Roberge, J. Vermette, S. Jandl, P. Fournier and M. M. Gospodinov, Magnetocaloric properties of the hexagonal HoMnO$_3$ single crystal revisited, *Phys. B*, 2015, **478**, 77–83, DOI: 10.1016/j.physb.2015.08.063.

17 E. Palacios, R. Sáez-Puche, J. Romero, Y. Doi, Y. Hinatsu and M. Evangelisti, Large magnetocaloric effect in EuGd$_2$O$_4$ and EuDy$_2$O$_4$, *J. Alloys Compd.*, 2022, **890**, 161847, DOI: 10.1016/j.jallcom.2021.161847.

18 A. Midya, N. Khan, D. Bhoi and P. Mandal, Giant magnetocaloric effect in magnetically frustrated EuHo$_2$O$_4$ and EuDy$_2$O$_4$ compounds, *Appl. Phys. Lett.*, 2012, **101**, 132415, DOI: 10.1063/1.4754849.

19 P. Mukherjee and S. E. Dutton, Enhanced Magnetocaloric Effect from Cr Substitution in Ising Lanthanide Gallium Garnets Ln$_3$CrGa$_4$O$_{12}$ (Ln = Tb, Dy, Ho), *Adv. Funct. Mater.*, 2017, **27**, 1701950, DOI: 10.1002/adfm.201701950.

20 N. K. Chogondahalli Muniraju, R. Baral, Y. Tian, R. Li, N. Poudel, K. Gofryk, N. Barišić, B. Kiefer, J. H. Ross and H. S. Nair, Magnetocaloric Effect in a Frustrated Gd-Garnet with No Long-Range Magnetic Order, *Inorg. Chem.*, 2020, **59**, 15144–15153, DOI: 10.1021/acs.inorgchem.0c02074.

21 Y. Tokiwa, S. Bachus, K. Kavita, A. Jesche, A. A. Tsirlin and P. Gegenwart, Frustrated magnet for adiabatic demagnetization cooling to milli-Kelvin temperatures, *Commun. Mater.*, 2021, **2**, 42, DOI: 10.1038/s43246-021-00142-1.

22 L. Li, K. Nishimura, W. D. Hutchison, Z. Qian, D. Huo and T. Namiki, Giant reversible magnetocaloric effect in $ErMn_2Si_2$ compound with a second order magnetic phase transition, *Appl. Phys. Lett.*, 2012, **100**, 152403, DOI: **10.1063/1.4704155**.

23 D. Guo, Y. Zhang, B. Wu, H. Wang, R. Guan, X. Li and Z. Ren, Structural, magnetic and magnetocaloric properties in $RE_2Ni_{1.5}Ga_{2.5}$ (RE = Dy, Ho, Er and Tm) compounds, *J. Alloys Compd.*, 2020, **830**, 154666, DOI: **10.1016/j.jallcom.2020.154666**.

24 J. W. Xu, X. Q. Zheng, S. X. Yang, L. Xi, D. S. Wang, C. F. Liu, J. Y. Zhang, Y. F. Wu, J. X. Shen, S. G. Wang and B. G. Shen, Large reversible magnetic entropy change of $R_3Ni_6Al_2$ (R = Dy, Ho and Er) compounds, *J. Alloys Compd.*, 2021, **879**, 160468, DOI: **10.1016/j.jallcom.2021.160468**.

25 S. Pakhira, C. Mazumdar, R. Ranganathan and M. Avdeev, Magnetic frustration induced large magnetocaloric effect in the absence of long range magnetic order, *Sci. Rep.*, 2017, **7**, 7367, DOI: **10.1038/s41598-017-07459-3**.

26 D. Jang, T. Gruner, A. Steppke, K. Mitsumoto, C. Geibel and M. Brando, Large magnetocaloric effect and adiabatic demagnetization refrigeration with $YbPt_2Sn$, *Nat. Commun.*, 2015, **6**, 8680, DOI: **10.1038/ncomms9680**.

27 D. N. Petrov, P. T. Long, Y. S. Koshkid'Ko, J. Ćwik and K. Nenkov, Large magnetocaloric effect in $LiLnP_4O_{12}$ (Ln = Gd, Tb, Dy) single crystals, *J. Phys. D: Appl. Phys.*, 2020, **53**, 495005, DOI: **10.1088/1361-6463/abb26f**.

28 A. Lukowiak, M. Stefanski, M. Ferrari and W. Strek, Nanocrystalline lanthanide tetraphosphates: energy transfer processes in samples co-doped with Pr^{3+}/Yb^{3+} and Tm^{3+}/Yb^{3+}, *Opt. Mater.*, 2017, **74**, 159–165, DOI: **10.1016/j.optmat.2017.03.025**.

29 N. Ben Hassen, M. Ferhi, K. Horchani-Naifer and M. Férid, Synthesis, characterization and optical properties of $LiSm(PO_3)_4$ phosphor, *Opt. Mater.*, 2015, **46**, 355–360, DOI: **10.1016/j.optmat.2015.04.045**.

30 B. Han, H. Liang, Y. Huang, Y. Tao and Q. Su, Luminescence of $LiTb(PO_3)_4:Sm^{3+}$ and energy transfer from Tb^{3+} to Sm^{3+} under vacuum ultraviolet-ultraviolet excitation, *Appl. Phys. B: Lasers Opt.*, 2011, **104**, 241–246, DOI: **10.1007/s00340-011-4580-6**.

31 H. Ettis, H. Naïli and T. Mhiri, The crystal structure, thermal behaviour and ionic conductivity of a novel lithium gadolinium polyphosphate $LiGd(PO_3)_4$, *J. Solid State Chem.*, 2006, **179**, 3107–3113, DOI: **10.1016/j.jssc.2006.06.003**.

32 D. N. Petrov, N. T. Dang, T. L. Phan, B. W. Lee, J. Ćwik, Y. S. Koshkid'ko, T. V. Manh, H. R. Park and S. C. Yu, Metamagnetism and Magnetocaloric Effect of $LiPr(PO_3)_4$ Crystal, *J. Electron. Mater.*, 2022, **51**, 4479–4485, DOI: **10.1007/s11664-022-09655-y**.

33 D. Petrov, B. Angelov and V. Lovchinov, Magnetic and XPS studies of lithium lanthanide tetraphosphates $LiLnP_4O_{12}$ (Ln=Nd, Gd, Er), *J. Rare Earths*, 2013, **31**, 485–489, DOI: **10.1016/S1002-0721(12)60307-X**.

34 C.-G. Ma, M. G. Brik, W. Ryba-Romanowski, H. C. Swart and M. A. Gusowski, Spectroscopy and Calculations for $4f^N \rightarrow$ $4f^{N-1}5d$ Transitions of Lanthanide Ions in K_3YF_6, *J. Phys. Chem. A*, 2012, **116**, 9158–9180, DOI: **10.1021/jp306409p**.

35 D. N. Petrov and B. M. Angelov, Fluorescence of UV-excited single crystals of $LiSmP4O12$ and $LiDyP_4O_{12}$, *Optik*, 2018, **169**, 291–296, DOI: **10.1016/j.ijleo.2018.05.080**.

36 N. Ben Hassen, M. Ferhi, K. Horchani-Naifer and M. Férid, Synthesis, characterization and optical properties of $LiSm(PO_3)_4$ phosphor, *Opt. Mater.*, 2015, **46**, 355–360, DOI: **10.1016/j.optmat.2015.04.045**.

37 B. M. Anghelov and B. M. Wanklyn, Flux growth of lithium rare-earth tetraphosphates, *J. Mater. Sci. Lett.*, 1986, **5**, 1067–1069, DOI: **10.1007/BF01730286**.

38 J. Rodríguez-Carvajal, Recent advances in magnetic structure determination by neutron powder diffraction, *Phys. B*, 1993, **192**, 55–69, DOI: **10.1016/0921-4526(93)90108-I**.

39 D. Zhao, F. Li, W. Cheng and H. Zhang, Lithium samarium polyphosphate, $LiSm(PO_3)_4$, *Acta Crystallogr., Sect. E: Struct. Rep. Online*, 2010, **66**, i3, DOI: **10.1107/S1600536809055822**.

40 S. Sebai, S. Hammami, A. Megriche, D. Zambon and R. Mahiou, Synthesis, structural characterization and VUV excited luminescence properties of $Li_xNa_{(1-x)}Sm(PO_3)_4$ polyphosphates, *Opt. Mater.*, 2016, **62**, 578–583, DOI: **10.1016/j.optmat.2016.11.015**.

41 M. B. Sanders, J. W. Krizan and R. J. Cava, $RE_3Sb_3Zn_2O_{14}$ (RE = La, Pr, Nd, Sm, Eu, Gd): a new family of pyrochlore derivatives with rare earth ions on a 2D Kagome lattice, *J. Mater. Chem. C*, 2016, **4**, 541–550, DOI: **10.1039/C5TC03798K**.

42 M. Ashtar, M. A. Marwat, Y. X. Gao, Z. T. Zhang, L. Pi, S. L. Yuan and Z. M. Tian, $REZnAl_{11}O_{19}$ (RE = Pr, Nd, Sm–Tb): a new family of ideal 2D triangular lattice frustrated magnets, *J. Mater. Chem. C*, 2019, **7**, 10073–10081, DOI: **10.1039/C9TC02643F**.

43 R. Higashinaka, A. Yamada, T. D. Matsuda and Y. Aoki, Relationship between specific heat, valence and effective magnetic moment of Sm ions in strongly correlated Sm compounds, *AIP Adv.*, 2018, **8**, 125017, DOI: **10.1063/1.5043120**.

44 S. Gupta, A. Das, K. G. Suresh, A. Hoser, Y. V. Knyazev, Y. I. Kuz'Min and A. V. Lukoyanov, Experimental and theoretical investigations on magnetic and related properties of ErRuSi, *Mater. Res. Express*, 2015, **2**, 046101, DOI: **10.1088/2053-1591/2/4/046101**.

45 E. Gamsjäger and M. Wiessner, Low temperature heat capacities and thermodynamic functions described by Debye–Einstein integrals, *Monatsh. Chem.*, 2018, **149**, 357–368, DOI: **10.1007/s00706-017-2117-3**.

46 B. K. Banerjee, On a generalised approach to first and second order magnetic transitions, *Phys. Lett.*, 1964, **12**, 16–17, DOI: **10.1016/0031-9163(64)91158-8**.

47 A. Arrott and J. E. Noakes, Approximate Equation of State For Nickel Near its Critical Temperature, *Phys. Rev. Lett.*, 1967, **19**, 786–789, DOI: **10.1103/PhysRevLett.19.786**.

48 A. Arrott, Criterion for ferromagnetism from observations of magnetic isotherms, *Phys. Rev.*, 1957, **108**, 1394–1396, DOI: **10.1103/PhysRev.108.1394**.

49 J. Zhou and G. A. Fiete, Rare earths in a nutshell, *Phys. Today*, 2020, **73**, 66–67, DOI: **10.1063/PT.3.4397**.

50 D. N. Petrov, V. Lovchinov, B. The Huy, P. The Long, N. T. Dang and D. S. Yang, Magnetic and cryogenic magnetocaloric properties of NaGdF$_4$ nanocrystals, *J. Appl. Phys.*, 2019, **126**, 135101, DOI: **10.1063/1.5114993**.

51 A. Midya, N. Khan, D. Bhoi and P. Mandal, Giant magnetocaloric effect in antiferromagnetic DyVO$_4$ compound, *Phys. B*, 2014, **448**, 43–45, DOI: **10.1016/j.physb.2014.03.019**.

52 D. X. Li, T. Yamamura, S. Nimori, Y. Homma, F. Honda and D. Aoki, Giant and isotropic low temperature magnetocaloric effect in magnetic semiconductor EuSe, *Appl. Phys. Lett.*, 2013, **102**, 152409, DOI: **10.1063/1.4802260**.

53 T. Samanta, I. Das and S. Banerjee, Giant magnetocaloric effect in antiferromagnetic ErRu$_2$Si$_2$ compound, *Appl. Phys. Lett.*, 2007, **91**, 152506, DOI: **10.1063/1.2798594**.